



## Data in Brief

## Genome-wide expression analysis comparing hypertrophic changes in normal and dysferlinopathy mice

Yun-Sil Lee<sup>a</sup>, C. Conover Talbot Jr.<sup>b</sup>, Se-Jin Lee<sup>a,\*</sup><sup>a</sup> Department of Molecular Biology and Genetics, Johns Hopkins University School of Medicine, 725 North Wolfe Street, PCTB 803, Baltimore, MD 21205, USA<sup>b</sup> Institute for Basic Biomedical Sciences, Johns Hopkins University School of Medicine, Baltimore, MD 21205, USA

## ARTICLE INFO

## Article history:

Received 14 October 2015

Accepted 18 October 2015

Available online 24 October 2015

## Keywords:

Myostatin

Follistatin

ACVR2B/Fc

Dysferlinopathy

Skeletal muscle

## ABSTRACT

Because myostatin normally limits skeletal muscle growth, there are extensive efforts to develop myostatin inhibitors for clinical use. One potential concern is that in muscle degenerative diseases, inducing hypertrophy may increase stress on dystrophic fibers. Our study shows that blocking this pathway in *dysferlin* deficient mice results in early improvement in histopathology but ultimately accelerates muscle degeneration. Hence, benefits of this approach should be weighed against these potential detrimental effects. Here, we present detailed experimental methods and analysis for the gene expression profiling described in our recently published study in Human Molecular Genetics (Lee et al., 2015). Our data sets have been deposited in the Gene Expression Omnibus (GEO) database (GSE62945) and are available at <http://www.ncbi.nlm.nih.gov/geo/query/acc.cgi?acc=GSE62945>. Our data provide a resource for exploring molecular mechanisms that are related to hypertrophy-induced, accelerated muscular degeneration in dysferlinopathy.

© 2015 The Authors. Published by Elsevier Inc. This is an open access article under the CC BY-NC-ND license (<http://creativecommons.org/licenses/by-nc-nd/4.0/>).

Specifications	
Organism/cell line/tissue	<i>Mus musculus</i> /quadriceps muscle
Sex	Male
Sequencer or array type	Affymetrix Mouse Exon 1.0 ST arrays
Data format	Raw data: CEL. Processed data: SOFT, MINiML, TXT.
Experimental factors	Genetically and pharmacologically induced muscular hypertrophy in normal vs. dysferlinopathy
Experimental features	Genome-wide expression analysis comparing hypertrophic changes in normal ( <i>wild-type</i> , <i>wt</i> ) and dystrophic ( <i>dysferlin</i> -deficient, <i>Dysf</i> <sup>-/-</sup> ) mouse muscles induced by genetic (follistatin overexpression, <i>F66</i> ) and pharmacological (administration of activin type II soluble receptor, ACVR2B/Fc) approaches
Consent	N/A
Sample source location	N/A

Genotype	ACVR2B/Fc treatment	Replicate	GEO accession URL
<i>wt</i>	No	3	<a href="http://www.ncbi.nlm.nih.gov/geo/query/acc.cgi?acc=GSM1536838">http://www.ncbi.nlm.nih.gov/geo/query/acc.cgi?acc=GSM1536838</a> <a href="http://www.ncbi.nlm.nih.gov/geo/query/acc.cgi?acc=GSM1536839">http://www.ncbi.nlm.nih.gov/geo/query/acc.cgi?acc=GSM1536839</a> <a href="http://www.ncbi.nlm.nih.gov/geo/query/acc.cgi?acc=GSM1536840">http://www.ncbi.nlm.nih.gov/geo/query/acc.cgi?acc=GSM1536840</a>
<i>wt</i>	Yes	3	<a href="http://www.ncbi.nlm.nih.gov/geo/query/acc.cgi?acc=GSM1536841">http://www.ncbi.nlm.nih.gov/geo/query/acc.cgi?acc=GSM1536841</a> <a href="http://www.ncbi.nlm.nih.gov/geo/query/acc.cgi?acc=GSM1536842">http://www.ncbi.nlm.nih.gov/geo/query/acc.cgi?acc=GSM1536842</a> <a href="http://www.ncbi.nlm.nih.gov/geo/query/acc.cgi?acc=GSM1536843">http://www.ncbi.nlm.nih.gov/geo/query/acc.cgi?acc=GSM1536843</a> <a href="http://www.ncbi.nlm.nih.gov/geo/query/acc.cgi?acc=GSM1536844">http://www.ncbi.nlm.nih.gov/geo/query/acc.cgi?acc=GSM1536844</a> <a href="http://www.ncbi.nlm.nih.gov/geo/query/acc.cgi?acc=GSM1536845">http://www.ncbi.nlm.nih.gov/geo/query/acc.cgi?acc=GSM1536845</a> <a href="http://www.ncbi.nlm.nih.gov/geo/query/acc.cgi?acc=GSM1536846">http://www.ncbi.nlm.nih.gov/geo/query/acc.cgi?acc=GSM1536846</a>
<i>Dysf</i> <sup>-/-</sup>	No	3	<a href="http://www.ncbi.nlm.nih.gov/geo/query/acc.cgi?acc=GSM1536847">http://www.ncbi.nlm.nih.gov/geo/query/acc.cgi?acc=GSM1536847</a> <a href="http://www.ncbi.nlm.nih.gov/geo/query/acc.cgi?acc=GSM1536848">http://www.ncbi.nlm.nih.gov/geo/query/acc.cgi?acc=GSM1536848</a> <a href="http://www.ncbi.nlm.nih.gov/geo/query/acc.cgi?acc=GSM1536849">http://www.ncbi.nlm.nih.gov/geo/query/acc.cgi?acc=GSM1536849</a>
<i>Dysf</i> <sup>-/-</sup>	Yes	3	<a href="http://www.ncbi.nlm.nih.gov/geo/query/acc.cgi?acc=GSM1536850">http://www.ncbi.nlm.nih.gov/geo/query/acc.cgi?acc=GSM1536850</a> <a href="http://www.ncbi.nlm.nih.gov/geo/query/acc.cgi?acc=GSM1536851">http://www.ncbi.nlm.nih.gov/geo/query/acc.cgi?acc=GSM1536851</a> <a href="http://www.ncbi.nlm.nih.gov/geo/query/acc.cgi?acc=GSM1536851">http://www.ncbi.nlm.nih.gov/geo/query/acc.cgi?acc=GSM1536851</a>
<i>F66</i>	No	3	<a href="http://www.ncbi.nlm.nih.gov/geo/query/acc.cgi?acc=GSM1536851">http://www.ncbi.nlm.nih.gov/geo/query/acc.cgi?acc=GSM1536851</a>

## 1. Direct link to deposited data

Raw and processed microarray data is available in GEO under accession GSE62945 <http://www.ncbi.nlm.nih.gov/geo/query/acc.cgi?acc=GSE62945>.

\* Corresponding author.  
E-mail address: [sjlee@jhmi.edu](mailto:sjlee@jhmi.edu) (S.-J. Lee).

(continued on next page)

(continued)

Genotype	ACVR2B/Fc treatment	Replicate	GEO accession URL
<i>F66;Dysf<sup>-/-</sup></i>	No	3	<a href="http://acc.cgi?acc=GSM1536852">acc.cgi?acc=GSM1536852</a> <a href="http://www.ncbi.nlm.nih.gov/geo/query/acc.cgi?acc=GSM1536853">http://www.ncbi.nlm.nih.gov/geo/query/acc.cgi?acc=GSM1536853</a> <a href="http://www.ncbi.nlm.nih.gov/geo/query/acc.cgi?acc=GSM1536854">http://www.ncbi.nlm.nih.gov/geo/query/acc.cgi?acc=GSM1536854</a> <a href="http://www.ncbi.nlm.nih.gov/geo/query/acc.cgi?acc=GSM1536855">http://www.ncbi.nlm.nih.gov/geo/query/acc.cgi?acc=GSM1536855</a>

## 2. Experimental design, materials and methods

### 2.1. Study design

The identification of myostatin as a negative regulator of skeletal muscle mass raised the possibility that blocking the myostatin signaling could have important applications for treating patients with muscle degenerative diseases [1]. However, there is one theoretical concern that inducing muscle hypertrophy may cause additional membrane stress,

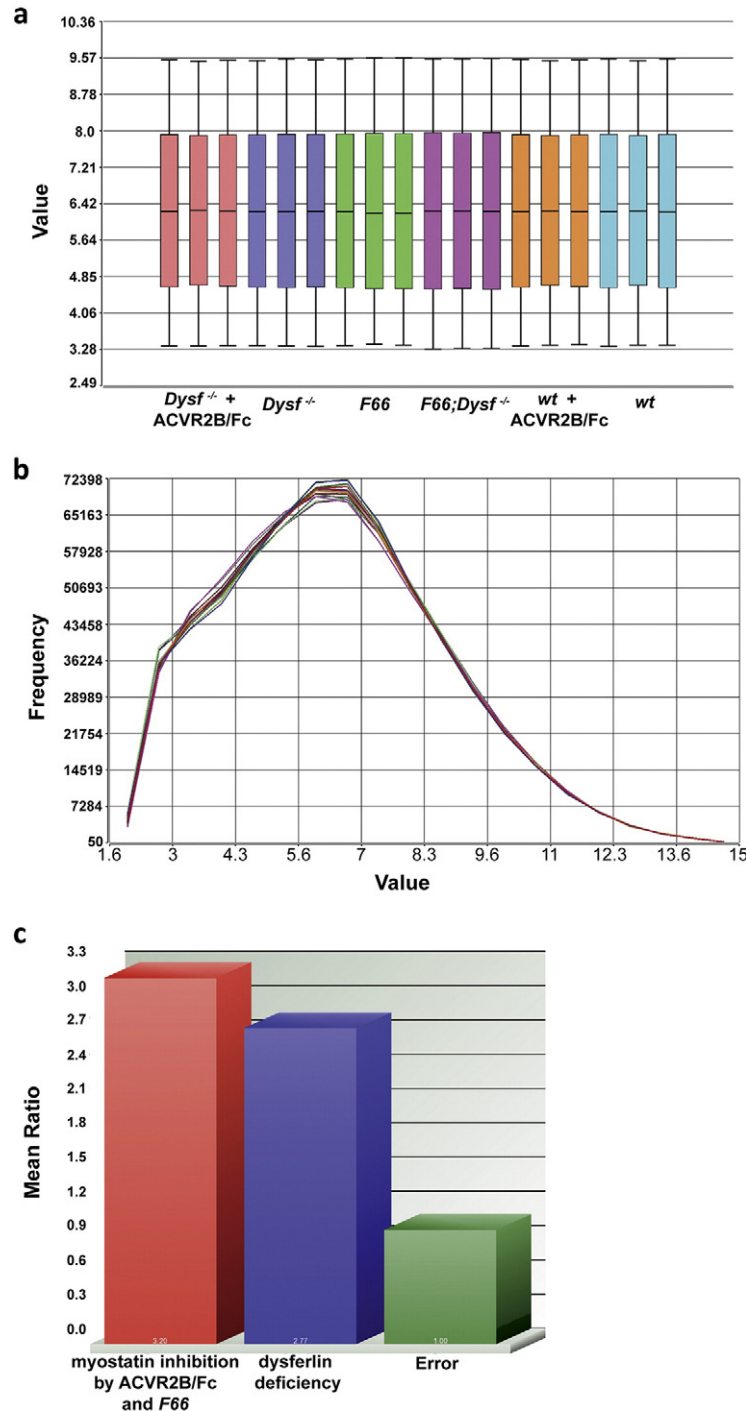


**Fig. 1.** Microarray quality assessment of 18 chips for three biological replicates in 6 different groups; *wt*, *Dysf<sup>-/-</sup>*, *F66*, *F66;Dysf<sup>-/-</sup>*, and ACVR2B/Fc-injected *wt* and *Dysf<sup>-/-</sup>* mice. (a) Box plots of 18 chips show median-centered raw data distributions. (b) Line graphs of 18 chips also support that all the chips' probes have signals of similar distribution and median value. (c) The magnitude of between class variation (myostatin inhibition by ACVR2B/Fc and *F66*, and dysferlin deficiency) is compared to that of within-class variation (Error), demonstrating biological variation to be far greater than experimental noise.

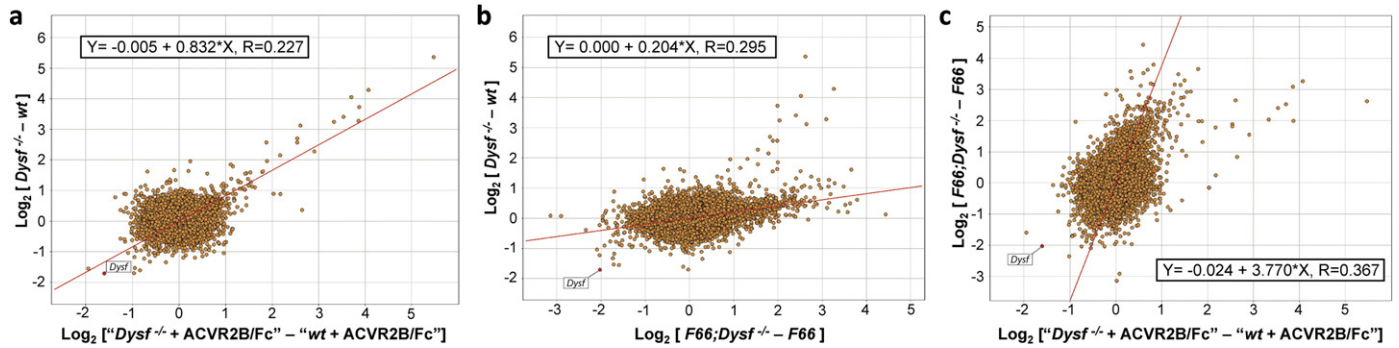


**Fig. 2.** QQ plots wherein one-way comparisons of transcriptome change are compared between different one-way comparisons. (a) “wt versus *Dysf*<sup>-/-</sup>” and “wt with ACVR2B/Fc versus *Dysf*<sup>-/-</sup> with ACVR2B/Fc”: most of the transcripts that are up-regulated in ACVR2B/Fc-injected *Dysf*<sup>-/-</sup> (versus wt with ACVR2B/Fc) are also up-regulated in *Dysf*<sup>-/-</sup> (versus wt). (b) “wt versus *Dysf*<sup>-/-</sup>” and “F66 versus F66;*Dysf*<sup>-/-</sup>”: most of the transcripts are up-regulated only in F66;*Dysf*<sup>-/-</sup> (versus F66). (c) “F66 versus F66;*Dysf*<sup>-/-</sup>” and “wt with ACVR2B/Fc versus *Dysf*<sup>-/-</sup> with ACVR2B/Fc”: most of the transcripts are up-regulated only in F66;*Dysf*<sup>-/-</sup> (versus F66). As expected, the probe set representing *Dysf* transcripts shows reduced hybridization with RNA from *Dysf*<sup>-/-</sup> (versus wt), ACVR2B/Fc-injected *Dysf*<sup>-/-</sup> (versus wt with ACVR2B/Fc), and F66;*Dysf*<sup>-/-</sup> (versus F66) muscles.

causing further damage to already fragile muscle fibers. To investigate this possibility, we used both genetic and pharmacological approaches to examine the effect of blocking myostatin in *dysferlin* mutant (*Dysf*<sup>-/-</sup>) mice, which is a model for limb-girdle type 2B and Miyoshi muscular dystrophies. Our rationale was that if myostatin inhibition

caused increased membrane damage, these effects would be enhanced in *Dysf*<sup>-/-</sup> mice, in which membrane repair is compromised [2]. For the genetic approach, we used transgenic mice expressing the myostatin inhibitor, follistatin, exclusively in skeletal muscle (*F66* transgenic mice) [3], and for the pharmacological approach, we used a soluble form of the activin type IIB receptor (ACVR2B) in which the extracellular ligand binding domain was fused to an Fc domain

**Table 1**

Top canonical pathways from Ingenuity Pathway Analysis (IPA).

Top canonical pathways	p-Value	Ratio
wt versus ACVR2B/Fc-injected wt		
Leptin signaling in obesity	1.14E-03	10/84 (0.119)
Cardiac β-adrenergic signaling	1.73E-03	14/158 (0.089)
G-protein coupled receptor signaling	5.04E-03	20/275 (0.073)
AMPK signaling	6.66E-03	13/169 (0.077)
Serotonin receptor signaling	6.79E-03	6/46 (0.130)
<i>Dysf</i> <sup>-/-</sup> versus ACVR2B/Fc-injected <i>Dysf</i> <sup>-/-</sup>		
PI3K/AKT signaling	5.37E-03	10/144 (0.069)
14-3-3-mediated signaling	9.88E-03	9/121 (0.074)
Role of Oct4 in mammalian embryonic stem cell pluripotency	1.1E-02	5/45 (0.111)
Assembly of RNA polymerase ii complex	1.69E-02	5/56 (0.089)
Complement system	1.84E-02	4/35 (0.114)
ACVR2B/Fc-injected wt versus ACVR2B/Fc-injected <i>Dysf</i> <sup>-/-</sup>		
IL-10 signaling	6.78E-04	9/78 (0.115)
Hepatic fibrosis/hepatic stellate cell activation	8.53E-04	13/146 (0.089)
TREM1 signaling	8.67E-04	8/71 (0.113)
Granulocyte adhesion and diapedesis	8.78E-04	15/178 (0.084)
Altered T cell and B cell signaling in rheumatoid arthritis	2.42E-03	9/92 (0.098)
wt versus F66		
Hepatic fibrosis/hepatic stellate cell activation	3.68E-07	22/146 (0.151)
Inhibition of matrix metalloproteases	1.22E-06	11/40 (0.275)
Glioma invasiveness signaling	3.21E-04	10/61 (0.164)
Granulocyte adhesion and diapedesis	4.49E-04	19/178 (0.107)
Coagulation system	9.15E-04	7/38 (0.184)
<i>Dysf</i> <sup>-/-</sup> versus F66; <i>Dysf</i> <sup>-/-</sup>		
Hepatic fibrosis/hepatic stellate cell activation	6.25E-16	36/146 (0.247)
Fcγ receptor-mediated phagocytosis in macrophages and monocytes	9.52E-15	29/102 (0.284)
Granulocyte adhesion and diapedesis	5.89E-12	35/178 (0.197)
Agranulocyte adhesion and diapedesis	6.81E-12	36/189 (0.190)
Leukocyte extravasation signaling	5.06E-10	35/207 (0.169)
F66 versus F66; <i>Dysf</i> <sup>-/-</sup>		
Fcγ receptor-mediated phagocytosis in macrophages and monocytes	2.4E-13	26/102 (0.255)
Dendritic cell maturation	1.82E-10	31/209 (0.148)
Leukocyte extravasation signaling	3.53E-10	33/207 (0.159)
Role of pattern recognition receptors in recognition of bacteria and viruses	3.7E-10	22/106 (0.208)
Hepatic fibrosis/hepatic stellate cell activation	1.09E-09	26/146 (0.178)

**Table 2**

Top upstream regulators from IPA.

Top upstream regulators	p-Value of overlap	Predicted activation state
wt versus ACVR2B/Fc-injected wt		
TNF	4.60E-08	
miR-141-3p (and other miRNAs w/seed AACACUG)	3.43E-07	
Lipopolysaccharide	5.11E-07	
Dexamethasone	9.34E-07	
GW501516	1.14E-06	
<i>Dysf</i> <sup>-/-</sup> versus ACVR2B/Fc-injected <i>Dysf</i> <sup>-/-</sup>		
miR-27a-3p (and other miRNAs w/seed UCACAGU)	1.78E-06	
miR-128-3p (and other miRNAs w/seed CACAGUG)	1.99E-06	
DYSF	6.04E-06	
miR-874-3p (and other miRNAs w/seed UGCCCUG)	1.29E-05	
miR-344d-3p (and other miRNAs w/seed AUAUAAAC)	3.15E-04	
ACVR2B/Fc-injected wt versus ACVR2B/Fc-injected <i>Dysf</i> <sup>-/-</sup>		
DYSF	1.42E-22	
Lipopolysaccharide	1.32E-20	Activated
IL1B	1.15E-17	Activated
TNF	2.06E-17	Activated
IL6	1.47E-13	Activated
wt versus F66		
TGFB1	8.48E-25	Activated
IL1B	3.48E-22	Activated
TNF	2.18E-20	Activated
Lipopolysaccharide	2.88E-20	Activated
Dexamethasone	7.91E-17	
<i>Dysf</i> <sup>-/-</sup> versus F66; <i>Dysf</i> <sup>-/-</sup>		
Lipopolysaccharide	2.80E-58	Activated
IFNG	1.31E-41	Activated
TNF	1.32E-39	Activated
TGFB1	1.57E-39	Activated
DYSF	2.23E-32	
F66 versus F66; <i>Dysf</i> <sup>-/-</sup>		
lipopolysaccharide	1.12E-44	Activated
TGFB1	7.23E-36	Activated
IFNG	8.84E-35	Activated
DYSF	3.05E-34	
TNF	5.02E-34	Activated

**Table 3**  
Top networks from IPA.

Top networks	Score
<i>wt</i> versus ACVR2B/Fc-injected <i>wt</i>	
Cell-mediated immune response, cellular development, cellular function and maintenance	65
Hematological system development and function, infectious disease, cell-mediated immune response	54
Gene expression, cell cycle, DNA replication, recombination, and repair	49
Cell signaling, molecular transport, vitamin and mineral metabolism	47
Lipid metabolism, molecular transport, small molecule biochemistry	43
<i>Dysf</i> <sup>-/-</sup> versus ACVR2B/Fc-injected <i>Dysf</i> <sup>-/-</sup>	
Hematological system development and function, gene expression, RNA post-transcriptional modification	87
Cellular compromise, molecular transport, nucleic acid metabolism	58
Cellular development, skeletal and muscular system development and function, cellular movement	52
Humoral immune response, protein synthesis, cell-to-cell signaling and interaction	52
Cardiovascular disease, cell morphology, cellular function and maintenance	51
ACVR2B/Fc-injected <i>wt</i> versus ACVR2B/Fc-injected <i>Dysf</i> <sup>-/-</sup>	
Increased levels of hematocrit, increased levels of red blood cells, inflammatory response	61
Cancer, cellular development, cellular growth and proliferation	60
Carbohydrate metabolism, lipid metabolism, small molecule biochemistry	53
Hematological system development and function, tissue morphology, inflammatory response	47
Developmental disorder, hereditary disorder, immunological disease	46
<i>wt</i> versus <i>F66</i>	
Small molecule biochemistry, cancer, gastrointestinal disease	70
RNA post-transcriptional modification, organismal development, renal and urological system development and function	63
Cellular movement, connective tissue disorders, cardiovascular disease	53
Lipid metabolism, small molecule biochemistry, molecular transport	52
Cell cycle, cardiovascular system development and function, embryonic development	50
<i>Dysf</i> <sup>-/-</sup> versus <i>F66</i> ; <i>Dysf</i> <sup>-/-</sup>	
Inflammatory response, cardiovascular system development and function, cardiovascular disease	58
Cancer, gastrointestinal disease, hepatic system disease	58
Connective tissue disorders, cellular assembly and organization, cellular function and maintenance	54
Cellular development, small molecule biochemistry, cell cycle	54
Cellular movement, hematological system development and function, immune cell trafficking	51
<i>F66</i> versus <i>F66</i> ; <i>Dysf</i> <sup>-/-</sup>	
Cellular assembly and organization, cell-to-cell signaling and interaction, cell death and survival	84
Cellular assembly and organization, cell cycle, connective tissue development and function	59
Cancer, reproductive system disease, neurological disease	55
Connective tissue disorders, dermatological diseases and conditions, developmental disorder	48
Cancer, dermatological diseases and conditions, hematological disease	48

(ACVR2B/Fc) [4]. Both follistatin and ACVR2B/Fc have been shown to increase muscle mass in mice.

## 2.2. Mice

To analyze the effect of *F66* in *Dysf*<sup>-/-</sup> mice, *F66* transgenic mice were mated with *Dysf*<sup>-/-</sup> mice. *F66*; *Dysf*<sup>+/-</sup> males from this cross were mated to *Dysf*<sup>+/-</sup> females to obtain *F66*; *Dysf*<sup>-/-</sup> and *F66*; *Dysf*<sup>+/+</sup> (= *F66*) males. Because the *F66* transgene is located on the Y chromosome, we focused all of our analysis on male mice. All mice were maintained on a C57BL/6 background. To analyze the effect of ACVR2B/Fc administration in *Dysf*<sup>-/-</sup> mice, male C57BL/6 (*wt*) and *Dysf*<sup>-/-</sup> mice beginning at 6 weeks of age were given four weekly intraperitoneal (i.p.) injections of either ACVR2B/Fc (10 mg kg<sup>-1</sup>, i.e., 200 µg per injection) or PBS.

## 2.3. Muscle tissues and RNA extraction

Total RNA was extracted from quadriceps muscles of 10 week old *wt*, *Dysf*<sup>-/-</sup>, *F66*, *F66*; *Dysf*<sup>-/-</sup>, and ACVR2B/Fc-injected *wt* and *Dysf*<sup>-/-</sup> mice (6 different groups), and three biological replicates were set up for each group. Quadriceps muscle (100 mg) was homogenized in TRIzol Reagent (Thermo Fisher Scientific Inc., Waltham, MA), and RNA was isolated from the supernatant with the RNeasy Mini Kit (Qiagen Inc., Valencia, CA), according to the manufacturer's instructions. All samples were treated with RNase-free DNase set (Qiagen Inc., Valencia, CA) to remove trace amounts of genomic DNA.

## 2.4. Labeling and hybridization

The Ambion Expression WT kit (Thermo Fisher Scientific Inc., Waltham, MA) was used to label isolated total RNA, according to the manufacturer's manual. The labeled cDNAs were hybridized onto Affymetrix Mouse Exon 1.0 ST arrays (Affymetrix, Inc., Santa Clara, CA) for 17 h at 45 °C with rotation (60 rpm) as described by Affymetrix in their GeneChip Expression Analysis Technical Manual. After washing, the arrays were scanned with Affymetrix' GeneChip Scanner 3000 7G.

## 2.5. Data processing

Affymetrix CEL files generated by GeneChip Command Console software were extracted and normalized using the Robust Multichip Analysis (RMA) algorithm in Partek Genomics Suite v6.6 software (Partek Inc., St. Louis, USA) [5]. To ensure exploration of the broadest range of gene transcripts, we imported all 641,130 Affymetrix "Extended Meta-probesets". Quality control assessments were run (Fig. 1) and these exon-level probesets were summarized into 115,830 transcripts, of which 34,343 currently had annotation at the gene level. As the understanding of genomics and information on the mouse genome increase these values will change over time, with the June 2015 annotation showing 47,252 gene-level transcripts.

Transcription analysis used a single expression value, determined from each transcript's exons, for transcript-level comparisons to detect differential gene expression between samples under different conditions. The one-way analysis of variance (ANOVA) was used to determine the magnitude (fold change) and statistical significance (*p*-value) of genes' changes in expression level between sample classes.

## 2.6. Data analysis

Microarray data were visualized by principal components analysis (PCA) mapping, volcano plots, and heat maps [6]. PCA analysis was performed with the Partek platform, while volcano plots and heat maps were generated with the Spotfire DecisionSite software (TIBCO Software Inc., Boston, MA). Linear regression analyses were performed with Spotfire to compare two different sets of transcriptome changes (Fig. 2). Gene Ontology (GO; [www.geneontology.org](http://www.geneontology.org)) analysis was conducted for significantly differentially expressed 763 genes (fold change >2.0, *p* < 0.01 in *wt* versus *F66*; *Dysf*<sup>-/-</sup>) using Spotfire's Gene Ontology Browser [7]. Canonical Pathways, Upstream Regulators, and Network analyses were generated using Ingenuity Pathway Analysis (IPA; QIAGEN Redwood City, CA, USA) and summarized in Tables 1, 2, and 3. Myostatin is a transforming growth factor-β (TGF-β) family member, and as expected, TGF-β1 was a top upstream regulator in *F66* mouse muscle (versus *wt*) (Fig. 3).

## 3. Conclusion

Collectively, our results demonstrated that *Fst* overexpression and ACVR2B/Fc administration in *dysferlin* mutant mice, a mouse model for limb-girdle type 2B and Miyoshi muscular dystrophies, induced

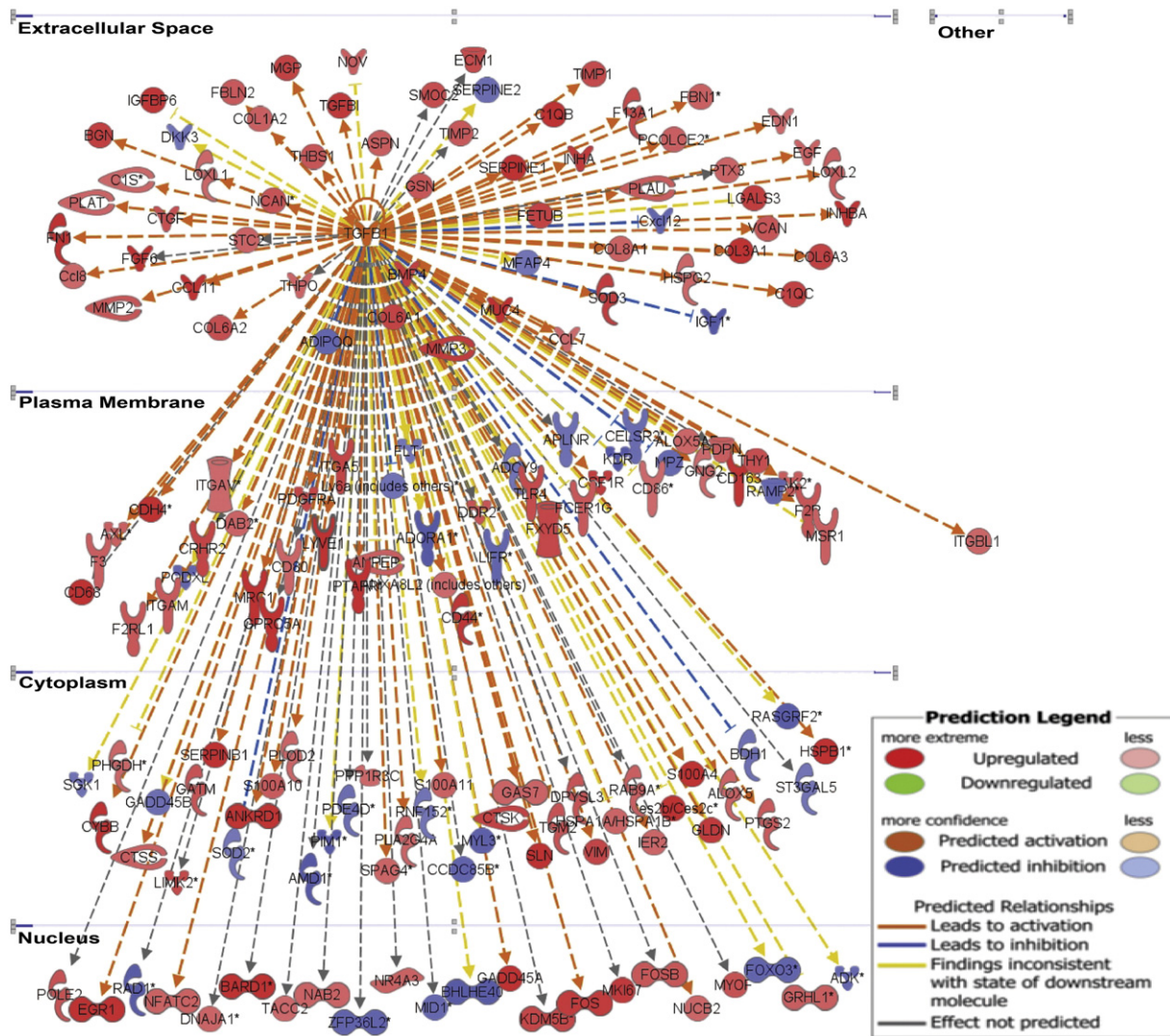


**Fig. 3.** Ingenuity upstream regulator analysis generated signaling-related networks based on published interactions with the top upstream regulator, TGFβ1, in F66 mouse muscle (versus wt) based on our experimental results. Red denotes upregulation, and blue denotes downregulation of the gene. The intensity of the gene color indicates the degree of up- or down-regulation. Orange lines indicate positive regulation, in accordance with the published interaction, blue lines indicate negative regulation, and yellow lines denote changes discordant from published expectation. The networks were generated through the use of Ingenuity Pathway Analysis.

the dramatic changes of gene expression profiling. Our data sets provide a resource for exploring molecular mechanisms that are related to hypertrophy-induced, accelerated muscular degeneration in dysferlinopathy.

**Funding**

This work was supported by the National Institutes of Health (grants to S.-J.L.: R01AR059685, R01AR060636, P01NS0720027). S.-J.L. was supported by generous gifts from Michael and Ann Hankin, Partners of Brown Advisory, and James and Julieta Higgins.

**Conflict of interest**

The authors declare that they have no conflicts of interest.

**References**

- [1] A.C. McPherron, A.M. Lawler, S.J. Lee, Regulation of skeletal muscle mass in mice by a new TGF-beta superfamily member. *Nature* 387 (1997) 83–90.
- [2] D. Bansal, K. Miyake, S.S. Vogel, S. Groh, C.C. Chen, R. Williamson, P.L. McNeil, K.P. Campbell, Defective membrane repair in dysferlin-deficient muscular dystrophy. *Nature* 423 (2003) 168–172.
- [3] S.J. Lee, A.C. McPherron, Regulation of myostatin activity and muscle growth. *Proc. Natl. Acad. Sci. U. S. A.* 98 (2001) 9306–9311.
- [4] S.J. Lee, L.A. Reed, M.V. Davies, S. Girgenrath, M.E. Goad, K.N. Tomkinson, et al., Regulation of muscle growth by multiple ligands signaling through activin type II receptors. *Proc. Natl. Acad. Sci. U. S. A.* 102 (2005) 18117–18122.
- [5] R.A. Irizarry, B.M. Bolstad, F. Collin, L.M. Cope, B. Hobbs, T.P. Speed, Summaries of Affymetrix GeneChip probe level data. *Nucleic Acids Res.* 31 (2003), e15.
- [6] Y.S. Lee, A. Lehar, S. Sebald, M. Liu, K.A. Swaggart, C.C. Talbot Jr., et al., Muscle hypertrophy induced by myostatin inhibition accelerates degeneration in dysferlinopathy. *Hum. Mol. Genet.* 24 (2015) 5711–5719.
- [7] J. Xiao, L. Jones-Brando, C.C. Talbot Jr., R.H. Yolken, Differential effects of three canonical *Toxoplasma* strains on gene expression in human neuroepithelial cells. *Infect. Immun.* 79 (2011) 1363–1373.